

## Small-Angle X-Ray-Scattering Study of Ordering Kinetics in a Block Copolymer

C. R. Harkless, M. A. Singh,<sup>(a)</sup> and S. E. Nagler

*Department of Physics, University of Florida, Gainesville, Florida 32611*

G. B. Stephenson and J. L. Jordan-Sweet

*IBM Thomas J. Watson Research Center, Yorktown Heights, New York 10598*

(Received 6 February 1990)

The kinetics of microphase separation and ordering of a diblock copolymer onto a lattice has been studied using time-resolved high-resolution small-angle x-ray scattering. The measurements show rapid formation of spherical domains after quenching and a subsequent ordering of the spheres. The results are discussed within the framework of simple models for nucleation and crystallization.

PACS numbers: 61.41.+e, 64.60.My, 64.60.Qb, 82.20.Mj

One of the foremost problems in statistical physics is the understanding of phase-transition kinetics.<sup>1-4</sup> There has been much recent progress in our understanding of the universal features of diverse phenomena such as phase separation and order-disorder transitions. The formation of an ordered lattice in block copolymers is unusual in that it involves a process with a conserved order parameter (microphase separation) as well as an ordering process with a nonconserved order parameter. Block copolymers are therefore novel systems for broadening our knowledge of kinetic phenomena.

Block copolymers are composed of two distinct polymer chains joined end to end by a covalent bond. When the block chains are incompatible the system will form mesophases of one chain within a background of the other chain below the dissolution temperature ( $T_d$ ). This is a fascinating variation of the phase separation seen in binary alloys involving the complex process of polymer interdiffusion with a constraint limiting the size of the phase-separated domains. For spherically shaped microdomains, ordering of the microdomains onto a lattice occurs below a second temperature  $T_o$ .<sup>5-7</sup> At intermediate temperatures between  $T_o$  and  $T_d$ , the positions of the spherical microdomains are weakly correlated, exhibiting short-range order as would be expected for a liquid or an amorphous solid. Since the equilibrium lattice structure is always observed upon cooling, it is natural to think of the intermediate states as a molecular liquid, the spherical domains being the "molecules." The ordering process at  $T_o$  is analogous to melting-crystallization phenomena.

The equilibrium properties of block copolymers have been well studied both theoretically<sup>8-12</sup> and experimentally.<sup>5,13-15</sup> There have also been important recent studies of the dynamics of the microphase separation.<sup>6,7,16,17</sup> In this Letter we report the results of a high-resolution time-resolved small-angle x-ray-scattering (SAXS) study of ordering kinetics in polystyrene (PS)-polybutadiene (PB) diblock copolymer (SB). The results show clearly that microphase separation proceeds rapidly

after a thermal quench, but ordering onto a lattice occurs on a distinctly slower time scale.

The SB used in this study was synthesized by Polymer Laboratories, Inc. The fractional composition was 29.5 wt% styrene, the molecular weight  $5.24 \times 10^4$ , and the polydispersity 1.04. In order to lower the transition temperature various solutions of the pure polymer in the selective solvent *n*-tetradecane (C14) were prepared. Under these conditions it is known that spherical microdomains of PS form within a PB-C14 matrix below  $T_d$ .<sup>5-7</sup>

The samples were placed in a quenching furnace equipped with Kapton windows.<sup>18</sup> X-ray-scattering measurements were performed at beam line X20C of the National Synchrotron Light Source.<sup>19</sup> The scattered photons were measured with a linear-silicon-diode-array position-sensitive detector. A tantalum beamstop blocked the direct beam, allowing measurement of the scattered profile in the range  $7.6 \times 10^{-3} - 1.1 \times 10^{-1} \text{ \AA}^{-1}$ . The measured full width at half maximum of the beam at zero angle was  $1 \times 10^{-3} \text{ \AA}^{-1}$ . The instrumental resolution does not play a significant role in the measurements presented here and is therefore ignored in the discussion below.

Before beginning the time-resolved experiments careful temperature-dependent static measurements were made. The important aspects are summarized here; a full account of the static experiments will be published elsewhere.<sup>18</sup> In agreement with the results of Hashimoto and co-workers<sup>5-7</sup> both  $T_d$  and  $T_o$  were clearly identifiable. The observed structures were thermally reversible. Bragg peaks characteristic of crystalline order appear below  $T_o$ , but coexist with short-range-order scattering indicating the persistence of a liquid or amorphous component. From considerations of volume fractions and the x-ray data the lattice structure in the ordered phase is easily identified as body-centered cubic (bcc). Previously the lattice structure has been reported as simple cubic.<sup>5-7</sup> It should be noted that the current experiment benefits from greatly improved resolution

TABLE I. Results of the temperature-dependent measurements.

wt% SB	$T_d$ (°C)	$T_o$ (°C)	Sphere radius (Å)	Lattice constant (Å)
25.0	155.0	101.0	93.4	468
35.0	165.0	107.0	97.9	446

and statistics. From theoretical considerations one expects to observe the bcc structure.<sup>8</sup> The results of the static studies are summarized in Table I.

The real-time measurements were performed as follows: The samples were annealed for approximately 20 min at a temperature  $T_i > T_d$ . The temperature was rapidly lowered to a final temperature  $T_f < T_o$  where it was kept fixed for the duration of the measurement. Quenches to within 1°C of the final temperature were typically achieved in 12–15 sec with no overshoot and a stability of  $\pm 0.3^\circ\text{C}$ . Scattering profiles were obtained sequentially with exposure times of 1–3 sec.

Typical results of a quench from 159.6 to 94.0°C for the 25 wt% SB in the C14 sample are shown in Fig. 1. Over the range 0.01–0.05 Å<sup>-1</sup>, the observed scattered intensity  $I(q)$  is dominated by three components:

$$I(q) = B(q) + |f(q)|^2 I^{\text{liq}}(q) + |f(q)|^2 I^{\text{sol}}(q), \quad (1)$$

where  $B(q)$  is the background which arises primarily from parasitic scattering by the Kapton windows.  $I^{\text{liq}}(q)$  and  $I^{\text{sol}}(q)$  are the liquid and crystalline structure factors, respectively, and  $f(q)$  is the form factor for the spherically shaped domains. The background contribution is measured directly and is a monotonically decaying function of  $q$  having a value of 100 counts/sec at the location of the main peak (the total scattered intensity at the same position is 6000 counts/sec). The second term in Eq. (1) is the result of interparticle interference from the microdomains which are in an amorphous or liquid-like state. The exact form for this scattering component is not known; however, the data were found to be well approximated by the sum

$$|f(q)|^2 I^{\text{liq}}(q) \approx A_0 \exp\left[-\frac{q^2}{2\sigma_0^2}\right] + A_1 \left[1 + \left(\frac{q-l_1}{\Gamma_1}\right)^2\right]^{-1} + A_2 \left[1 + \left(\frac{q-l_2}{\Gamma_2}\right)^2\right]^{-1}. \quad (2)$$

We note that a model used successfully to predict the scattering from liquid argon<sup>20,21</sup> can be accurately represented with this parametrization. This component is shown in Fig. 1 as a dashed line. The third term in Eq. (1) represents the ordered contribution and shows up as

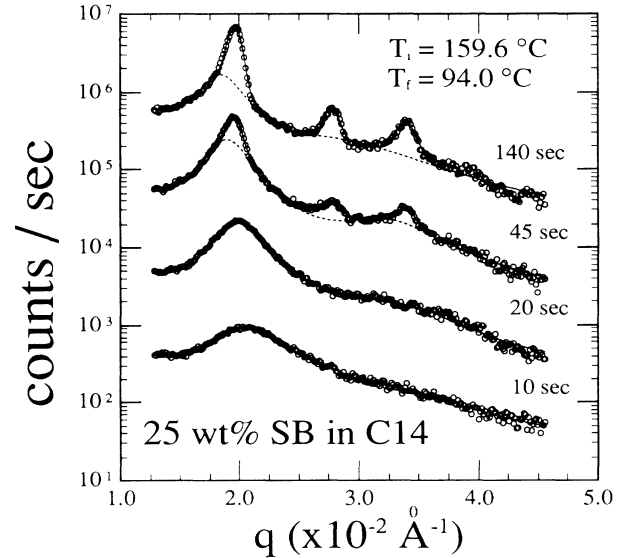


FIG. 1. Results of a typical quench as described in the text. The counting times are 1 sec per spectrum. The spectra are offset by factors of 10 for clarity. The solid lines are fits to the data using Eq. (1). The dotted lines represent the contribution from the liquid portion of the scattering as described by Eq. (2).

Bragg peaks in the scattered spectrum. The Bragg peaks are characterized by a sum of Gaussians:

$$|f(q)|^2 I^{\text{sol}}(q) \approx \sum_{i=1}^3 G_i \exp\left[-\frac{(q-b_i)^2}{2\sigma_i^2}\right], \quad (3)$$

with the restrictions  $b_2 = \sqrt{2}b_1$  and  $b_3 = \sqrt{3}b_1$ . The scattering from the first-order Bragg peak is easily discernible from the broad Lorentzian peak upon which it is superposed. The raw data were fitted by the sum of the three terms in Eq. (1) and the result is shown as a solid line in Fig. 1.

Figure 2 shows the maximum value of the scattered intensity in the region of the first-order Bragg reflection  $[(1.5-2.75) \times 10^{-2} \text{Å}^{-1}]$  following a quench from 159.6 to 94.0°C on the 25 wt% sample and typifies all of the quench data. These values are taken directly from the raw spectra and clearly show that there are two distinct regimes for the transformation kinetics. The temperature profile is also included in Fig. 2 and shows that while the process of microdomain formation occurs rapidly as the temperature is lowered, the ordering process occurs isothermally at a much later time.

The widths of the Bragg peaks show little or no change with time. On the other hand, the fitted width of the Lorentzian peaks decreases rapidly immediately after the quench, and reaches a nearly constant value near the onset of ordering.

Figure 3 shows the fitted amplitudes of the first liquid peak and the first-order Bragg peak as a function of time following the quench. The liquid peak grows rapidly so

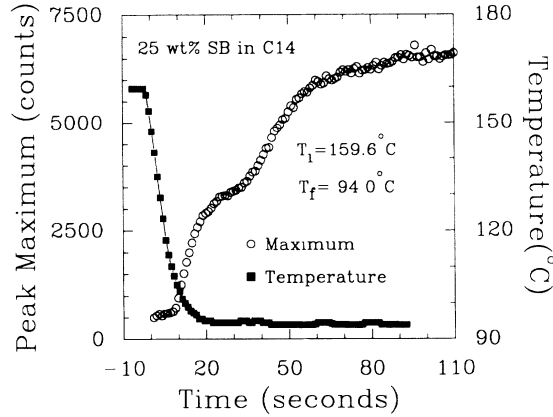


FIG. 2. Typical results for the maximum value of the scattered intensity in the vicinity of the principle peak as a function of time after the quench. The solid line through the temperature profile is a guide to the eye.

that the spherical domains are clearly evident by the time the temperature has reached  $T_f$ . At later times the liquid peak begins to decay as the first-order Bragg amplitude grows, indicating that regions of long-range order are beginning to form. The final state is seen to be a coexistence of the liquidlike and crystalline regions.

The measured intensity  $I(t)$  of a Bragg reflection is proportional to the fraction of material in the crystalline state,  $\zeta$ . The widths of the Bragg peaks exhibit little or no change with time, so  $\zeta$  is proportional to the peak height. The Mehl-Johnson-Avrami (MJA) steady-state nucleation theory<sup>22-24</sup> predicts that the fraction of material in the ordered state  $\zeta$  should grow as

$$\zeta = (1 - e^{-bt^n}), \quad (4)$$

where for a constant nucleation rate  $n=4$ . This should be valid at early times, and as seen in Fig. 3, the early-time data are well represented by this form. The late-time growth is slower, and is fitted well by a pure exponential [ $n=1$  in Eq. (4)], also shown in Fig. 3. This crossover is evident in all of the quench data. A best fit to the whole range of data (see Fig. 3) with  $n$  varying yields a growth exponent of 3.66. The data clearly deviate from this form, especially at late times. The apparent slowing of growth at late times may arise from the effects of site saturation and impingement, which are accounted for in the theory discussed below.

Cahn<sup>22,25</sup> (C) derived a relation which describes nucleation occurring on two-dimensional defects. The model assumes a constant isotropic growth velocity. The resulting expression for the Bragg-peak intensity can be written as

$$I(t) = I_\infty (1 - e^{-bf(t-t_0)}), \quad (5)$$

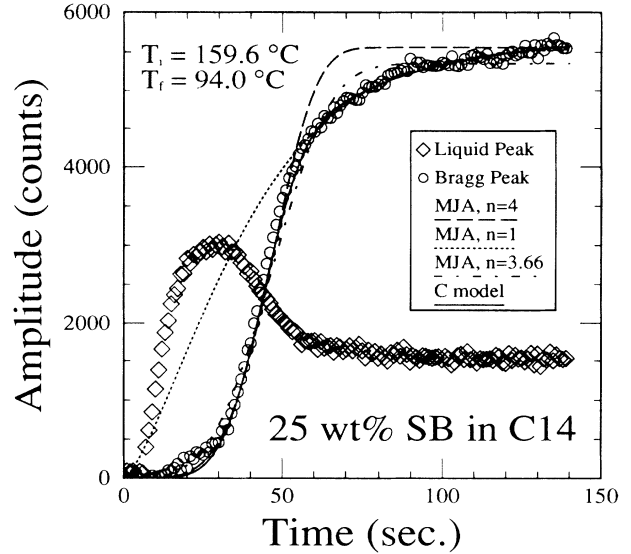


FIG. 3. Fitted values for the first-order liquid and first-order Bragg-peak amplitudes as a function of time after the quench for the same quench as shown in Figs. 1 and 2. The Bragg-peak amplitude is fitted by simple models for nucleation as discussed in the text. Dashed line: fit to the early-time data using Eq. (4) with  $n=4$ . Dotted line: fit to the late-time data using Eq. (4) with  $n=1$ . Dash-dotted line: fit of the full range of the data by Eq. (4) with  $n$  allowed to vary. Solid line: fit by Eq. (5).

where

$$f(t) = (t/a) \int_0^1 [1 - \exp\{(-\pi/3)(t/a)^3 \times (1 - 3\xi^2 + 2\xi^3)\}] d\xi. \quad (6)$$

At early times  $f(t) \sim t^4$ ; at late times  $f(t) \sim t$ . The nucleation rate, which typically has a sigmoidal shape,<sup>23</sup> is approximated here as a step function which is zero during the incubation time  $t_0$  and a nonzero constant after  $t_0$ . The fit parameters  $a$  and  $b$  depend on the growth velocity, the surface area available for nucleation, and the steady-state nucleation rate.

The solid line in Fig. 3 is a fitted by this model with variable parameters  $a$ ,  $b$ ,  $t_0$ , and  $I_\infty$ . The model fits the data very well for all times. From the late-time limit of Eqs. (5) and (6), it is apparent that the quantity  $\tau = a/b$  plays the role of an effective time constant. Table II gives the effective time constants for the C model. It is seen that there is a minimum in the time constants at intermediate quench depths. Larger time constants in the deep quench limit are a consequence of reduced thermal activation. Larger time constants in the shallow quench limit are a signature of a "critical" slowing down which arises from a smaller free-energy difference between the phases. The detailed dependence of the ordering process on quench depth is still under investigation.

TABLE II. Fitted time constants.

25 wt% SB, $T_i = 160^\circ\text{C}$		35 wt% SB, $T_i = 170^\circ\text{C}$	
$T_f$ ( $^\circ\text{C}$ )	$\tau$ (sec)	$T_f$ ( $^\circ\text{C}$ )	$\tau$ (sec)
94.0	32.2	102.2	89.1
89.5	30.7	94.0	23.1
84.0	26.6	86.5	19.3
75.0	33.9	82.0	24.6
67.0	49.8	70.5	28.6
57.0	81.2	58.7	205.1

These data are extremely interesting in that both the  $n=4$  and  $n=1$  limits of the standard nucleation and growth models are observed. Typically the nucleation rate is either too high so that site saturation occurs early and the whole range appears as a pure exponential, or the nucleation rate is too low so that the site saturation occurs late in the transformation and only MJA behavior with  $n=4$  is seen.

The question arises as to whether there are indeed two-dimensional defects present which act as nucleation sites. One may speculate that the surface of an impurity particle of micron size or greater may act in the same way as such a defect. There is, however, at present no direct information about the type and number of impurities in the specimens.

In summary, we have carried out time-dependent small-angle x-ray-scattering measurements of the ordering kinetics in a block copolymer system. The transition from a homogeneous state to a microphase-separated and then ordered state has been observed. The scattering profiles show the existence of regions of liquid and bcc crystalline correlations between the spherical domains. The ordering kinetics are well described by Cahn's model for defect-induced nucleation, including the effect of site saturation. The system is ideal for studying the full range of time dependence in this model. A full and detailed account of these results will be published elsewhere.<sup>18</sup>

Useful discussions with M. Sutton, M. Burns, and R. F. Shannon, Jr., were greatly appreciated. Outstanding technical assistance was provided by Ward Ruby. This research was supported by the U.S. Department of Energy (Office of Basic Energy Sciences) under award No.

DE-FG05-86ER45280. The National Synchrotron Light Source is supported by the U.S. Department of Energy, Division of Material Sciences and Division of Chemical Sciences (Contract No. DE-AC02-76CH00016).

(a)Current address: Queen's University, Kingston, Ontario, Canada K7L 3N6.

<sup>1</sup>J. G. Gunton, M. San Miguel, and P. S. Sahni, in *Phase Transitions and Critical Phenomena*, edited by C. Domb and J. Lebowitz (Academic, New York, 1983), Vol. 8, p. 267.

<sup>2</sup>K. Binder, Rep. Prog. Phys. **50**, 783 (1987).

<sup>3</sup>G. F. Mazenko *et al.*, Phys. Rev. B **31**, 4453 (1985).

<sup>4</sup>G. F. Mazenko and O. T. Valls, Phys. Rev. B **30**, 6732 (1984).

<sup>5</sup>M. Shibayama *et al.*, Macromolecules **16**, 16 (1983).

<sup>6</sup>T. Hashimoto *et al.*, Macromolecules **19**, 750 (1986).

<sup>7</sup>T. Hashimoto *et al.*, Macromolecules **18**, 754 (1986).

<sup>8</sup>L. Leibler, Macromolecules **13**, 1602 (1980).

<sup>9</sup>A. Chakrabarti *et al.*, Phys. Rev. Lett. **63**, 2661 (1989).

<sup>10</sup>T. Ohta and K. Kawasaki, Macromolecules **19**, 2621 (1986).

<sup>11</sup>K. Kawasaki *et al.*, Macromolecules **21**, 2972 (1988).

<sup>12</sup>H. Matsuoka *et al.*, Phys. Rev. B **36**, 1754 (1987).

<sup>13</sup>T. Hashimoto *et al.*, Macromolecules **13**, 1660 (1980).

<sup>14</sup>F. S. Bates *et al.*, Macromolecules **15**, 589 (1982).

<sup>15</sup>T. Hashimoto *et al.*, Macromolecules **16**, 361 (1983).

<sup>16</sup>K. Kawasaki and K. Sekimoto, Physica (Amsterdam) **148A**, 361 (1988).

<sup>17</sup>Y. Oono and M. Bahiana, Phys. Rev. Lett. **61**, 1109 (1988).

<sup>18</sup>C. R. Harkless, M. A. Singh, S. E. Nagler, G. B. Stephenson, and J. L. Jordan-Sweet (to be published).

<sup>19</sup>G. B. Stephenson, Nucl. Instrum. Methods Phys. Res., Sect. A **266**, 477 (1988).

<sup>20</sup>A. Guinier and G. Fournet, *Small Angle Scattering of X-Rays* (Wiley, New York, 1955).

<sup>21</sup>G. Fournet, C. R. Acad. Sci. (Paris) **228**, 1071 (1949).

<sup>22</sup>J. W. Christian, *The Theory of Transformation in Metals and Alloys, Part 1: Equilibrium and General Kinetic Theory* (Pergamon, New York, 1981).

<sup>23</sup>M. Avrami, J. Chem. Phys. **7**, 1103 (1939); **8**, 212 (1940); **9**, 177 (1941).

<sup>24</sup>W. A. Johnson and R. F. Mehl, Trans. Am. Inst. Min. Metall. Eng. **135**, 416 (1939).

<sup>25</sup>J. W. Cahn, Acta Metall. **4**, 449 (1956).